# Ancient Water on Asteroid 4 Vesta: Evidence from a Quartz Veinlet in the Serra de Magé Eucrite Meteorite

Allan H. Treiman [a*], Antonio Lanzirotti [b], and Dimitrios Xirouchakis [c].

[a] Lunar and Planetary Institute, 3600 Bay Area Blvd., Houston TX 77058 U.S.A..

[b] Consortium for Advanced Radiation Sources, University of Chicago at Brookhaven National Laboratory, Upton, NY 11973, USA

[c] Johnson Space Center, Bldg. 31, Houston, TX 77058, USA

* Corresponding Author.

Email Addresses: treiman@lpi.usra.edu (A. Treiman), lanzirotti@bnl.gov (A. Lanzirotti), dxirouch@email.msn.com (D. Xirouchakis)

Manuscript. May 15, 2003.

Key Words: Water, 4 Vesta, quartz vein, eucrite (meteorite type), Serra de Magé (meteorite name), polar ice.

**The meteorite Serra de Magé, a eucrite inferred to be from the asteroid 4 Vesta, contains quartz veinlets. They are identical to antitaxial or "crack-seal" quartz veinlets in terrestrial rocks, and are extraterrestrial and ancient because they pre-date a 4.40 Ga metamorphism. The quartz was likely deposited from liquid water solutions (as are terrestrial veins); other potential solvents or transport mechanisms are inadequate or unlikely. Because the is no indication of internal (magmatic) water in the eucrite meteorites and thus in Vesta, the water from which the veinlet was deposited probably came from outside Vesta. By analogy with water ice deposits on the Moon and Mercury, Vesta and similar asteroids may have had (or now have) polar ice deposits, possibly derived from comet impacts.**

## Introduction

The distribution of water in the early solar system is important for understanding its evolution, the evolution of its planetary bodies, and the formation of life and pre-biotic chemical compounds. Water has also been critical in formulating plans for solar system exploration, including the current emphasis on Mars and Europa [1,2]. Similarly, the presence of water ice on nominally anhydrous planetary bodies [3-5] suggests that water may be available in many previously unexpected environments in the solar system. Here, we document a likely sign of water in a meteorite from another nominally anhydrous body – the asteroid 4 Vesta.

The meteorite Serra de Magé, focus of this work, belongs to the 'HED' clan of basaltic achondrites [6]: E = eucrites, basalts; D = diogenites, cumulate orthopyroxenites derived from basaltic magma; and H = howardites, breccia mixtures of eucrite and diogenite fragments. These meteorites are inferred to be related because of close similarities in chemistry and isotopic composition [6]. The close correspondence between reflectance spectra of the HED meteorites and those of the asteroid 4 Vesta suggest that the HEDs originated on Vesta [7,8].

The Serra de Magé meteorite fell to Earth in 1923 and was collected shortly thereafter [9]. It is a cumulate, formed by accumulation of pyroxenes and plagioclase within a eucritic basalt magma [10]. Serra de Magé consists mostly of plagioclase feldspar and orthopyroxene with exsolution lamellae of augite (Fig. 1a); minor minerals include tridymite, chrome spinel, ilmenite, troilite, iron metal [11], and (reported here) quartz. The plagioclase and pyroxene

occur in mm- to cm-sized grains in anastomosing intergrowths [12]. Other mineral grains are scattered among and within the plagioclase and pyroxene. Tridymite (a $SiO_2$ polymorph) occurs as rare mm-sized grains among the pyroxene and plagioclase, and as spongy intergrowths with augite, plagioclase and chrome spinel. The former represent late magmatic crystals, and the latter probably represent mesostasis – relics of late-stage magma.

Serra de Magé is ancient. Its crystallization is not known with certainty, but is probably near 4.55 Ga like other eucrites [13]. Serra de Magé was metamorphosed intensely, as shown by the chemical homogeneity of its minerals [11,12,14]. Chemical compositions of its coexisting augite and orthopyroxene (Table 1) imply Fe-Mg-Ca equilibration at 1100±60 K [15]. This metamorphic event is recorded in the meteorite's radiochronometer ages; the U-Th-Pb system give 4.40±0.035 Ga [16], which is consistent with less precise ages from the Rb-Sr and Sm-Nd systems [16,17].

## Methods

Mineral chemical analyses were obtained by electron microprobe (Cameca SX-100) at Johnson Space Center, Houston, TX. Analyses were by normal techniques for silicate minerals: electron accelerating potential of 15 kV, focussed beam, and beam current of 10 nA into a Faraday cup. Standards were well-characterized minerals and synthetic materials, and data reduction used the $\phi$-$\rho$-z algorithm supplied by Cameca.

Synchrotron X-ray micro-diffraction (SXRD) analyses were obtained with the hard X-ray microprobe, X26A, National Synchrotron Light Source, Brookhaven National Laboratory [18]. For these analyses, the synchrotron X-ray emissions from the NSLS X26A bending magnet are first collimated and monochromated. For the experiments reported here, the X-ray wavelength was tuned to 0.72084Å to coincide with the commonly used MoK$\alpha$ X-rays. Other experiments used different wavelengths with identical results. The 350 µm x 350 µm collimated X-ray beam is focused to a 10-µm diameter at the thin section location using a system of Rh coated, Kirckpatrick-Baez type microfocusing mirrors. However the thin section itself is held at 45° to the incident X-ray beam, so the beam impinges onto the thin section in an ellipse of ~ 10 x 15 µm. These SXRD experiments are in transmission mode – diffracted X-rays pass through the sample to the detector. Since it was not readily feasible to remove the section from the glass slide for this experiment, the diffractions thus represent grains in the

thin section plus its glass substrate. Separate analysis of the glass confirms that it is amorphous.

Diffracted X-rays were imaged in a Bruker SMART 1500 CCD camera with a 4:1 fiber optic taper, in high-resolution mode at 1024x1024 pixels (96 μm pixel size). The camera was located so that the X-ray beam center (undiffracted X-rays) was just off of the CCD array. The distance between the camera and the thin section was adjusted for convenience. A sample of dispersed powdered corundum ($\alpha$-$Al_2O_3$, NIST SRM 674a) provided a reference for defining the camera position and correction for any spatial distortions within the array. A diffraction pattern of that corundum sample was taken, and modeled using the free-ware computer code FIT2D [19] to yield best fit values for the camera-sample distance, the camera tilt and rotation, and the beam center on the camera plane. Experimental parameters in the experiments reported here are given in Table 2; identical results were obtained in other experiments at different camera positions.

The images show diffraction spots from crystalline phases, and a broad diffuse diffraction centered at d≈3.5Å from the borosilicate glass substrate for the thin section. The diffraction images shown below have had the diffuse glass diffraction removed by subtracting a scaled diffraction image from the glass alone. Scaling was needed because the intensity of the synchrotron X-ray beam decreases with time.

For areas with many small mineral grains, the SXRD images show circles of diffractions, like Debye-Scherrer patterns (Figure 1). Most single crystals show only diffuse scattering, as they are not at a diffracting orientation with respect to the X-ray beam. Single crystals at diffracting conditions show portions of reciprocal lattice nets – lines or grids of spots representing diffracted beams. This is to be expected given that the analyses are being done *in-situ* and that the crystal domain size may vary relative to the diameter of the focused beam. SXRD diffraction images were integrated to yield graphs of diffracted intensity versus d spacing using the computer code FIT2D [19].

To validate the application of SXRD to meteorites in thin section, we obtained diffraction images for tridymite, plagioclase, and orthopyroxene grains near the silica veinlet. Tridymite diffractions are consistent with the low-temperature monoclinic polymorph [20] (Figure 3). Plagioclase diffractions (Fig. 4) are consistent with anorthite [21], the plagioclase in Serra de Magé (Table 1, [9,11,12]). Pyroxene diffractions (Fig. 4) are consistent with orthopyroxene having the lattice parameters measured for that mineral in Serra de Magé [14],

and as calculated for its chemical composition [21] (Table 1). In fine-grained samples, relative intensities of diffractions were generally consistent with tabulated values.

## Quartz Veinlets

As part of a larger study of the eucrite meteorite Serra de Magé, we discovered veinlets of a silica mineral in thin section AMNH 3786-5 (Fig. 1), from the American Museum of Natural History. The silica was initially identified by its optical properties (parallel extinction, low birefringence, and low index of refraction) and confirmed by electron microprobe chemical analysis (Table 1). Optically, the silica is length-slow. The biggest veinlet (Fig. 1) can be followed piecewise along a fracture or microfault plane for ~1 cm – the width of the thin section. The longest continuous segment of the veinlet is ~2 mm long, where the veinlet reaches its maximum width of ~100 μm (Fig. 1b,c). The veinlet is commonly ~50 μm wide, and pinches to nothing in spots. The veinlet cuts across grains of pyroxene and plagioclase, and rarely follows grain boundaries. The core of the silica veinlet is marked by a line or septum of grains (a few μm across) of pyroxene and plagioclase, even where one or the other mineral are not at the veinlet's wall (Fig. 1b-d, Fig. 4). The septum is commonly at the geometric center of the veinlet, but also may be offset to either side. Where the veinlet is thickest, the septum is a solid mass of mineral fragments (Fig. 1b,c). In scattered locations within the veinlets are small round opaque inclusions, probably iron sulfide (by reflected light microscopy), which form short rows parallel to the walls of the veinlets (Fig. 1c).

The silica mineral in the veinlet was identified *in situ* in the thin section to be α-quartz by microbeam synchrotron X-ray diffraction. The X-ray diffraction image and its integration (Fig. 2) show a ring of strong diffractions, consistent with many grains of a single mineral species (Fig. 1). The diffraction at d=3.36Å is by far the strongest in the pattern, and is consistent with α-quartz, for which the strongest diffraction is nominally at 3.34Å, and for which other diffractions are <20% as intense [21]. The observed pattern is inconsistent with those of other silica polymorphs, especially of the tridymite found elsewhere in the meteorite (Fig. 3). The other low-pressure polymorphs of silica would be recognizable because their most intense diffractions are at higher d values than α-quartz (high-tridymite, 4.37Å; low-tridymite, 4.33Å; high-cristobalite, 4.05Å; low-cristobalite, 4.14Å; keatite, 4.49 Å). These other silica polymorphs have diffractions besides their strongest that could have been detected

(e.g., more than 50% as intense as the strongest diffraction) but were not. Similarly, the observed peaks are inconsistent with any of the high-pressure polymorphs of silica [18].

The quartz grains of the veinlet are roughly columnar and perpendicular to the margins of the veinlet, and some are continuous across the whole width of the veinlet (Fig. 1b, d). Many quartz columns maintain near-constant widths across the veinlet. Rarely, a quartz column appears to be truncated outward by another column, yielding a slight increase in average column width outward.

Several smaller quartz veinlets occur within 1 mm of the largest veinlet. These smaller veinlets are narrower than ~30 μm width, and up to 1 mm long. One is enclosed entirely in the pyroxene grain of Figure 1, and another fills a grain boundary between a pyroxene and a plagioclase.

The quartz veinlets must be ancient and therefore extraterrestrial, because they formed before Serra de Magé was metamorphosed. Evidence that the veinlets are ancient is textural. First, augite exsolution lamellae in the orthopyroxene terminate (or begin) at the quartz veinlet (Fig. 1b, d). The veinlet must pre-date the exsolution lamellae, or the veinlet would crosscut the lamellae. The chemical compositions of the exsolution lamellae equilibrated during the metamorphism that is correlated (above) with the 4.40 Ga radiochronologic age. Second, where the veinlet thins to zero width in the pyroxene, the pyroxene is healed across the veinlet trace – optically continuous without sign of the original fracture or microfault (Fig. 1d). This indicates that the pyroxene was annealed after the veinlet was deposited, and the annealing can be attributed to the 4.40 Ga metamorphism.

## Comparison With Terrestrial Quartz Veins

All the features of the quartz veinlets in Serra de Magé are found in a common type of quartz vein in terrestrial rocks. These are the so-called antitaxial or "crack-seal" veinlets [22], which grow by successive deposition of material at their margins [22-25], not by infilling of an open cavity in the rock. Mineral grains near the vein centers, i.e. the septum (Fig. 1b,c,d), are relict fragments from the initial formation of a vein's crack (i.e., fault gouge). The first quartz deposited in an antitaxial vein is that closest to the center or the septum – the quartz becomes younger and younger away from the center or septum. On Earth, antitaxial veins occur principally in low-grade metamorphic rocks, where they represent silica mobility during brittle deformation.

The quartz veinlets in Serra de Magé share the following features with terrestrial "crack-seal" veinlets: columnar grains of quartz, continuous across the veinlet's center; quartz columns not coarsening toward the center; textures suggesting growth from the middle outward; a central region (septum) of fragments of wall minerals (here, pyroxene and plagioclase); and discontinuous lines of mineral inclusions parallel to the veinlet walls (Fig. 1d) [22-25]. The veinlets are not the chalcedony or agate varieties of quartz [26] because their grains are optically length slow. The veinlets did not form by filling open cracks because: their quartz grains are not inward-directed bundles or hemispheres of fibers; their quartz grains do not coarsen inwards; the veinlets' centers do not show quartz euhedra; and the centers do not contain other water-deposited minerals (e.g. clays) or their metamorphosed equivalents (e.g., micas or aluminosilicates).

## Mobility of Silica

To form the quartz veinlets in Serra de Magé, silica must have been transported to, and deposited at, the veinlet margins. Antitaxial quartz veins on Earth are assumed or inferred to have been deposited from water solutions. For the veinlets in the Serra de Magé meteorite, it is important to consider whether some other solvent or agent might be possible.

Silica can be transported in, and deposited by, water-rich vapors. Silica is fairly common in vesicles of volcanic rocks (both basaltic and rhyolitic) and as vapor-mediated alterations of volcanic rocks [27,28]. However, the silica phase under these circumstances is tridymite (less commonly, cristobalite) and rarely quartz.

Little silica can dissolve in carbon dioxide vapor or fluid, so it is unlikely as a transport medium. In mixed $H_2O$-$CO_2$ fluid, silica solubility declines precipitously with increasing $CO_2$ content. In fact, available data are consistent with zero silica solubility in pure $CO_2$ [29]. In the eucrites themselves, their rare vesicles (as in Ibitira) may represent $CO_2$-CO vapor [30], but contain no vapor-deposited silica [31]. Similarly, vesicles in lunar basalts probably represent CO-$CO_2$ vapors [32], and contain no vapor-deposited silica [33,34].

Finally, silica is not likely to be mobile without a solvent or carrier gas, because its vapor pressure is extremely low. Thermochemical calculations imply that the pressure of $SiO_2$(g) over silica ranges from ~$10^{-53}$ bars at 500K to ~$10^{-17}$ bars at 1200K (data from [35]). This low vapor pressure seems to preclude significant chemical transport. Deposition from SiO(g) is also unlikely. In strict disproportionation of solid silica to SiO(g) + 1/2 $O_2$(g), the

partial pressure of SiO(g) is calculated to be as insignificant as that of $SiO_2$(g). If SiO(g) had been generated by other means (e.g., a reaction like $Fe^0 + 2SiO_2 = FeSiO_3$ (pyroxene) + SiO(g)), oxygen must have been available at the veinlet sites to for solid quartz from that gas. However, there is no evidence that oxygen was removed from other phases near the veinlets (i.e., iron metal is not concentrated near the quartz veinlets).

Several eucrites show evidence of post-igneous (or late igneous) chemical transport, though not of silica alone. Post-igneous transport of iron is suggested by iron-enrichment along cracks in igneous pyroxenes in several eucrites, commonly with iron-rich olivine in the cracks (NWA1000 [36]; Pasamonte, [37], pers. obs.), Similarly, several polymict eucrite breccias contain olivine and silica fragments rimmed by pyroxene [38,39]. These textures seem best explained by iron mobility, not silica mobility (*contra* [39]). Tabular veinlets or dikelets rich in tridymite occur in another eucrite [40], and are inferred to represent differentiated silicate magma.

Thus, aqueous solutions appear to be the most likely transport agents in forming quartz veins like that in Serra de Magé and on Earth. For Serra de Magé, this inference is difficult to confirm independently. The quartz veinlets are not associated with other indications of aqueous solutions, i.e., hydrous minerals (e.g., micas, or chlorites), their metamorphic dehydration products, or other water-deposited minerals (e.g., sulfates or carbonates). Of course, their terrestrial "crack-fill" counterparts are rarely associated with such minerals either.

## Source Of Water

If these quartz veinlets were deposited by aqueous solutions, before 4.40 Ga on the asteroid 4 Vesta, it seems unlikely that the water was indigenous. No high-temperature water-bearing minerals (e.g., H-bearing apatite or amphibole) have been reported from any HED meteorite [6]. Low-temperature hydrous minerals (e.g., clays, serpentine) are also unknown except in exotic clasts of carbonaceous chondrite materials [41,42]. Thus, there is no direct evidence of water in the HED basalts, basaltic cumulates, or mantle. Similarly, the igneous evolution of the eucrite meteorites can be explained entirely by anhydrous magmas [43].

Lacking an internal source, it is likely that the veinlet's water was external – arriving on Vesta after the eucrite basalts had formed. Water could have been derived from hydrous meteorite fragments in the regolith [41,42] and mobilized during an impact metamorphic

event. Water could also have been derived from solar wind hydrogen, implanted into regolith breccias (e.g., the Kapoeta and Jodzie howardites [44,45]). Or, water could have come from impacting comets [46]. It may be impossible to distinguish among these alternatives, as the intense metamorphism that Serra de Magé experienced [14] would have erased isotopic clues to the origins of the water or silica.

## Implications

Evidence for liquid water on 4 Vesta, early in the history of the solar system, has important implications for the mobility and availability of water. While water is present in many asteroids (inferred from meteorite studies and reflectance spectra) and from 'dead' comets masquerading as asteroids, it is generally assumed that their water is indigenous and accumulated along with the asteroid. The quartz veinlets in Serra de Magé provide evidence that water was deposited on asteroids after accretion, and thus that a significant quantity of water was mobile in the asteroid belt between 4.55 and 4.40 Ga (the igneous formation and metamorphism ages of Serra de Magé).

This suggestion of exogenous water on Vesta parallels recent findings of polar ice deposits on other nominally anhydrous bodies: the Moon and Mercury [3-5]. Mechanisms for accumulating polar ice deposits can operate (and could have operated) throughout the solar system [47,48], and there is no obvious reason that the same mechanisms could not operate in the asteroid belt. Polar ices now in the inner solar system may derive mostly from large comets [47], and that may also have been true in the asteroid belt early in the solar system. If so, asteroids like Vesta may also have received prebiotic organic molecules from the comets [48] – and may have had the internal heat for continued prebiotic chemical reactions (as shown by the strong metamorphism of Serra de Magé). The presence of water ice on Vesta may be tested later this decade, if the proposed *Dawn* spacecraft mission and its neutron spectrometer are selected for flight [49].

## Acknowledgments

For the loan of thin sections, we are grateful to: the American Museum of Natural History (J. Bosenberg), the Smithsonian Museum of Natural History (T. McCoy), and the University of New Mexico Institute of Meteoritics (R. Jones). C. Schwandt and K. Goldman

assisted with EMP analyses; we are grateful to NASA/JSC for use of that instrument. Some petrographic data were developed during a Lunar and Planetary Institute Summer Internship in 2001 to K. Goldman. The computer program FIT2D® [19] is graciously provided *gratis* by A. Hammersly and European Synchrotron Research Facility (ERSF). We are grateful to D. Wiltschko, L.P. Knauth, and P. Heaney for informative discussions on the properties and formation of quartz veins. Treiman's support is from LPI CAN funds and NASA grants NAG5-8270 and NAG5-12184. Xirouchakis was supported by NASA grant NCC 980 to B.L.Wilson and by Mrs. Irini Kotelou. Micro-SXRD studies at NSLS beamline X26A are supported by DOE grant DOEFG0292ER14244 to S. Sutton, M. Rivers, and A. Lanzirotti (CARS/U. Chicago). Research carried out in part at the National Synchrotron Light Source, Brookhaven National Laboratory, which is supported by the U.S. Department of Energy, Division of Materials Sciences and Division of Chemical Sciences, under Contract No. DE-AC02-98CH10886. Reviews from C. Herd, A. Reid, and [your name here] were helpful. Lunar and Planetary Institute Contribution #1xxx.

## References

[1] W.V. Boynton, W.C. Feldman, S.W. Squyres, T. Prettyman, J. Brückner, L.G. Evans, R.C. Reedy, R. Starr, J.R. Arnold, D.M. Drake, P.A.J. Englert, A.E. Metzger, I. Mitrofanov, J.I. Trombka, C. d'Uston, H. Wänke, O. Gasnault, D.K. Hamara, D.M. Janes, R.L. Marcialis, S. Maurice, I. Mikheeva, G.J. Taylor, R. Tokar, and C. Shinohara, Distribution of hydrogen in the near-surface of Mars: Evidence for sub-surface ice deposits. Science 297 (2002) 81-85.

[2] R.T. Pappalardo, M.J.S. Belton, H.H. Breneman, J.H. Carr, C.R. Chapman, G.C. Collins, T. Denk, S. Fagents, P.E. Geissler, B. Geise, R. Greeley, R. Greenberg, J.W. Head, P. Helfenstein, G. Hoppa, S.D. Kadel, K.P. Klaasen, J.E. Klemaszewski, K. Magée, A.S. McEwen, J.M. Moore, W.B. Moore, G. Neukum, C.B. Philips, L.M. Procter, G. Schubert, D.A. Senske, R.J. Sullivan, B.R. Tufts, E.P. Turtle, R. Wagner, and K.K. Williams, Does Europa have a subsurface ocean? Evaluation of the geological evidence. J. Geophys. Res. 104 (1999) 24015-24055.

[3] S. Nozette, C.L. Lichtenberg, P.D. Spudis, R. Bonner, W. Ort, E. Malaret, M. Robinson, and E.M. Shoemaker, The Clementine bistatic radar experiment, Science 274 (1996) 1495-1498.

[4] W.C. Feldman, S. Maurice, A.B. Binder, B.L. Barraclough, R.C. Elphic, and D.J. Lawrence, Fluxes of fast and epithermal neutrons from Lunar Prospector: Evidence for water ice at the lunar poles. Science 281 (1998) 1496-1500.

[5] M.A. Slade, B.J. Butle, D.O. Muhleman, Mercury radar imaging: Evidence for polar ice. Science 258 (1992) 635-640.

[6] D.W. Mittlefehldt, T.J. McCoy, C.A. Goodrich, A. Kracher, Non-chondritic meteorites from asteroidal bodies, ch 4. in J.J. Papike (Ed.), Planetary Materials (Rev. Mineral. 36) Mineral. Soc. Amer., Washington DC, (1998).

[7] G.J. Consolmagno, M.J. Drake, Composition and evolution of the eucrite parent body: Evidence from rare earth elements. Geochim. Cosmochim Acta 41 (1978), 1271-1282.

[8] M.J. Drake, The eucrite/Vesta story. Meteor. Planet. Sci. 36 (2001) 501-513.

[9] C.B. Gomes, K. Keil, Brazilian Stone Meteorites, Univ. New Mexico, Albuquerque (1980) 161 p.

[10] A.H. Treiman, The parent magmas of the cumulate eucrites: A mass balance approach, Meteor. Planet. Sci. 32 (1997) 217-230.

[11] M. Prinz, C.E. Nehru, J.L. Berkley, K. Keil, C.B. Gomes, Petrogenesis of the Serra de Magé cumulate eucrite (abstr.), Meteoritics 12 (1977) 341.

[12] A.H. Treiman, K. Goodman, Petrology of the cumulate eucrite Serra De Magé. Lunar Planet. Sci. XXXIII, Lunar and Planetary Institute, Houston, (2002) Abstract #1191.

[13] M.I. Smoliar, A survey of Rb-Sr systematics of eucrites, Meteoritics 28 (1993) 105-113.

[14] G.E. Harlow, C.E. Nehru, M. Prinz, G.J. Taylor, K. Keil, Pyroxenes in Serra de Magé: Cooling history in comparison with Moama and Moore County, Earth Planet. Sci. Lett. 43 (1979) 143-181.

[15] D.J. Andersen, D.H. Lindsley, P.M. Davidson, QUILF: a PASCAL program to assess equilibria among Fe-Mg-Mn-Ti oxides, pyroxenes, olivine, and quartz, Computers & Geosciences 19 (1993) 1333-1350.

[16] F. Tera, R.W. Carlson, N.Z. Boctor, Radiometric ages of basaltic achondrites and their relation to the early history of the solar system, Geochim. Cosmochim. Acta 61 (1997) 1713-1731.

[17] S.B. Jacobsen, G.J. Wasserburg, Sm-Nd isotopic evolution of chondrites and achondrites, II, Earth Planet. Sci. Lett. 67 (1984) 137-150.

[18] D. Xirouchakis, D.S. Draper, C.S. Schwandt, A. Lanzirotti, Crystallization conditions of Los Angeles, a basaltic Martian meteorite, Geochim. Cosmochim. Acta 66 (2002) 1867-1880.

[19] A.P. Hammersley, FIT2D V10.3 Reference Manual V4.0. European Synchrotron Research Facility, Paper ESRF98HA01T (1998). (program and manual available at http://www.esrf.fr/computing/expg/subgroups/data_analysis/FIT2D/)

[20] W.A. Dollase, W.H. Baur, The superstructure of meteoritic low tridymite solved by computer simulation. Amer. Mineral. 61 (1976), 971-978.

[21] I.Y. Borg, D.K. Smith, Calculated X-ray Powder Patterns for Silicate Minerals. Geol. Soc. Amer. Memoir 122, Geol. Soc. Amer., Boulder CO. (1969), 896 p.

[22] J.G. Ramsay, The crack-seal mechanism of rock deformation, Nature 284 (1980) 135-139.

[23] D.V. Wiltschko, J.W. Morse, Z.D. Sharp, W.M. Lamb, Analysis of veins in low temperature environments: Introduction for structural geologists, Geol. Soc. America, 1998 Ann. Mtg. short course (1998) 97 p.

[24] P.D. Bons, The crack-seal mechanism of rock deformation, J. Virtual Explorer **2** (Stress, Strain and Structure, A Volume in Honour of W.D. Means. Eds: M.W. Jessell and J.L.Urai.) http://www.virtualexplorer.com.au/VEjournal/2000Volumes/Volume2/www/contribs/bons/text/2_1.html (2000).

[25] D.V. Wiltschko, J.W. Morse, Crystallization pressure versus “crack seal” as the mechanism for banded veins, Geology 29 (2001) 79-82.

[26] H. Graetsch, Structural characteristics of opaline and microcrystalline silica minerals, in P.J. Heaney, C.T. Prewitt, G.V. Gibbs (Eds.) Silica – Physical Behavior, Geochemistry, and Materials Applications, (Rev. Mineral. 29), Mineral. Soc. Amer., Washington DC (1994) ch. 6.

[27] W.A. Deer, R.A. Howie, J. Zussman, Rock Forming Minerals Vol. 4 Framework Silicates, Longmans Green & Co. Ltd., London. (1963), 435 p.

[28] J.W. Anthony, R.A. Bideaux, K.W. Bladh, M.C. Nichols, Handbook of Mineralogy Volume II - Silica and Silicates. Mineralogical Society America, Washington DC. (1995). <http://www.minsocam.org/MSA/Handbook/>

[29] R.C. Newton, C.E. Manning, Quartz solubility in $H_2O$-NaCl and $H_2O$-$CO_2$ solutions at deep crust-upper mantle pressures and temperatures: 2 – 15 kbar and 500 – 900°C, Geochim. Cosmochim. Acta 64 (2000) 2993-3003.

[30] T.J. McCoy, L. Wilson, G.K. Benedix, R.A. Ketcham, M. Wadhwa, A.M. Davis, Vesicular eucrites: Where and how did they form and why are they so rare? (abstract). Lunar Planet. Sci. XXXIV, Lunar and Planetary Institute, Houston (2003) Abstract #1187.

[31] M. Wadhwa, A.M. Davis, Vapor deposited mineral assemblages in vesicles of the eucrite Ibitira (abstract). Lunar Planet. Sci. XXIX, Lunar and Planetary Institute, Houston (1998) Abstract #1931.

[32] G.J. Taylor, P. Warren, G. Ryder, J. Delano, C. Pieters, G. Lofgren, Lunar Rocks, p. 183-284 in Lunar Sourcebook (eds. G.H. Heiken, D.T. Vaniman, B.M. French). Cambridge University, New York (1991).

[33] H.H. Schmitt, G. Lofgren, G.A. Swann, G. Simmons, The Apollo 11 samples: An introduction. p. 1-54 in Proc. Apollo 11 Lunar Sci. Conf., Pergamon (1970).

[34] J.W. Frondel, Lunar Mineralogy, J. Wiley & Sons, New York (1975) 323 p.

[35] M.W. Chase (Ed.), NIST-JANAF Thermochemical Tables, Fourth Edition. Monograph No. 9 of J. Phys. Chem. Ref. Dat., Amer. Inst. Phys., Woodbury NY, (1998) 1950 p.

[36] P. Warren, Northwest Africa 1000: A new eucrite with maskelynite, unequilibrated pyroxene crisscrossed by fayalite-rich veins, and Stannern-like geochemistry (abstr.), Lunar Planet. Sci. XXXIII, (2002) Abstract #1147.

[37] J.M. Schwartz, I. S. McCallum, F. Camara, C. Domeneghetti and M. Zema, Pasamonte eucrite: Subsolidus thermal history (abstr), Lunar Planet. Sci. XXXIII, (2002) Abstract #1147.

[38] T. Labotka T., J.J. Papike, Howardites: Samples of the the eucrite parent body: Petrology of Frankfort, Pavlovka, Yurtuk, Malvern, and ALHA 77302, Proc. Lunar Planet. Sci. Conf. 11th, (1980) 1103-1130.

[39] A.H. Treiman, M.J. Drake, Basaltic volcanism on the eucrite parent body: Petrology and chemistry of the polymict eucrite ALHA80102. Proc. Lunar Planet. Sci. Conf. 15th, J. Geophys. Res. 90 Suppl., (1985) C619-C628.

[40] D.W. Mittlefehldt and M.T. Lee, Petrology and geochemistry of unusual eucrite GRA 98098 (abstr.), Meteorit. Planet. Sci. 36, (2001) A136.

[41] M.E. Zolensky, R.H. Hewins, D.W. Mittlefehldt, M.M. Lindstrom, X. Xiao, M.E. Lipschutz, Mineralogy, petrology and geochemistry of carbonaceous chondritic clasts in the LEW 85300 polymict eucrite, Meteoritics 27 (1992) 596-604.

[42] M.E. Zolensky, M.K. Weisberg, P.C. Buchanan, D.W. Mittlefehldt, Mineralogy of carbonaceous chondrite clasts in HED achondrites and the moon, Meteor. Planet. Sci. 31 (1996) 518-537.

[43] E.M. Stolper, Experimental petrology of eucrite meteorites, Geochim. Cosmochim. Acta 51 (1977) 587-611.

[44] L. Schulz, H. Kruse, Helium, neon, and argon in meteorites – A data compilation, Meteoritics 24 (1989) 155-172.

[45] R.L. Palma, R.H. Becker, R.O. Pepin, D.J. Schlutter, Irradiation records in regolith materials, II: Solar wind and solar energetic particle components in helium, neon, and argon extracted from single lunar mineral grains and from the Kapoeta howardite by stepwise pulse heating, Geochim. Cosmochim. Acta 66 (2002) 2929-2958.

[46] J. Teemu, T. Mäkinen, J.-L. Bertaux, M.R. Combi, E. Quémerais, Water production of Comet C/1999 S4 (LINEAR) Observed with the SWAN Instrument, Science 292 (2001) 1326-1329.

[47] J.I. Moses, K. Rawlins, K. Zahnle, L.Dones, External sources of water for Mercury's putative ice deposits, Icarus 137 (1999) 197-221.

[48] C.F. Chyba, C. Sagan, Comets as a source of prebiotic organic molecules for the early Earth, , p. 147-173 in P.J. Thomas, C.F. Chyba, C.P. McKay (Eds.), Comets and the Origin and Evolution of Life, Springer, N.Y., (1997).

[49] C.T. Russell, A. Coradini, W.C. Feldman, R. Jaumann, A.S. Konopliv, T.B. McCord, L.A. McFadden, H.Y. McSween, S. Mottola, G. Neukum, C.M. Pieters, C.A. Raymond, D.E. Smith, M.V. Sykes, B.G. Williams, M.T. Zuber, Dawn: A journey to the beginning of the solar system, Proc. Asteroids Comets Meteors Conf. 2002. Available at <http://www-ssc.igpp.ucla.edu/dawn/pdf/ACMConferencePaper.pdf>

Table 1. Average chemical compositions of minerals in Serra de Magé, by electron microprobe.

| | Quartz in veinlet | Tridymite* | Augite | Ortho-pyroxene | Plagio-clase |
|---|---|---|---|---|---|
| $SiO_2$ | 96.64 | 97.35 | 51.22 | 50.15 | 43.93 |
| $TiO_2$ | 0.05 | 0.05 | 0.28 | 0.20 | 0.01 |
| $Al_2O_3$ | 0.02 | 0.04 | 0.59 | 0.40 | 36.28 |
| $Cr_2O_3$ | 0.01 | 0.05 | 0.23 | 0.15 | 0.01 |
| FeO | 0.39 | 0.30 | 10.23 | 26.38 | 0.15 |
| MnO | 0.02 | 0.02 | 0.41 | 0.91 | 0.01 |
| MgO | 0.01 | 0.01 | 13.42 | 18.26 | 0.00 |
| CaO | 0.02 | 0.04 | 22.07 | 1.02 | 19.70 |
| $Na_2O$ | 0.01 | 0.00 | 0.05 | 0.04 | 0.50 |
| $K_2O$ | 0.02 | 0.01 | 0.00 | 0.01 | 0.01 |
| Sum | 97.21 | 97.89 | 98.52 | 97.54 | 100.60 |

* Intergrown with augite (see text).

Table 2. Experimental Conditions for SXRD

| | | |
|---|---|---|
| X-ray wavelength | λ | 0.72084 Å |
| Camera - Sample Distance * | d | 191.4 mm |
| Camera Rotation Angle * | r | -43.283° |
| Camera tilt angle * | t | 1.792° |
| Beam Center – x * | | 1024.43 pixels |
| Beam Center – y * | | 482.29 pixels |

*Refined from diffraction pattern of corundum standard with computer code FIT2D® [19].

## Figure Captions

Figure 1. Quartz veinlets in the Serra de Mage meteorite, thin section AMNH 3786-5 (American Museum of Natural History). Crossed polarized light except as noted. [a]. Largest quartz veinlet (V) cutting pyroxene (Px) and plagioclase (Pl). [b] Detail of thickest portion quartz veinlet. Central septum (S) of pyroxene and plagioclase fragments. Some quartz columns (dark and light stripes) extend across the full width of the veinlet (arrow). Augite exsolutions (Au) in the pyroxene terminate at the veinlet. [c] Same scene, plane-polarized light. Central septum (S), and line of opaque inclusions (arrow) parallel to veinlet wall. [d] One end of the largest quartz veinlet. The pyroxene (yellow-orange) is completely healed around the veinlet end to upper left of image (optically continuous, no fracture evident). Dark line running right to left across image is a crack. Some quartz columns (dark and light stripes) extend across the full width of the veinlet (arrow).

Figure 2. Synchrotron X-ray diffraction data for the quartz vein of Figure 1, after subtraction of diffraction from the thin section glass (see methods). [a] Diffraction image, reversed contrast (dark spots are high X-ray intensity). Coordinate numbers are corrected pixel locations on the CCD camera; center of direct beam is near middle of right-hand edge of image (Table 2). Prominent ring of sharp diffractions suggests that the target is randomly oriented grains of a single mineral. The d value for this ring is consistent with the strongest diffraction of α-quartz, Qz {101}. [b] Integration of this image into d values (by FIT2D® [19]). The four strongest peaks of this 'powder-X-ray diffraction pattern' can all be attributed to α-quartz [21]: {101} at d=3.34Å; {110} at d=2.45Å; {102} at d=2.30Å; and {112} at d=1.82 Å. Miller indices are for hexagonal setting: $\{a_1a_2c\}$.

Figure 3. Synchrotron X-ray diffraction data for a tridymite grain near the quartz veinlet in Serra de Magé, after subtraction of diffraction from the thin section glass (see methods). The grain was identified optically by its very low birefringence and patchy subgrains and twins. [a] Diffraction image, reversed contrast (dark spots are high X-ray intensity). Coordinate numbers are corrected pixel locations on the CCD camera; center of direct beam is near middle of right-hand edge of image (Table 2). Target consists of two or three subgrains close to a diffracting condition, so the image shows isolated spots. [b] Integration of this image into

d values (by FIT2D® [19]). Most of the peaks of this 'powder-X-ray diffraction pattern,' though weak, can be attributed to monoclinic low-temperature tridymite [20] as annotated. The remaining peaks can be attributed to pyroxene and/or plagioclase.

Figure 4. Synchrotron X-ray diffraction data for the fine-grained dark patch at the center of the quartz vein (Fig. 1b,c), after subtraction of diffraction from the thin section glass (see methods). [a] Diffraction image, reversed contrast (dark spots are high X-ray intensity). Coordinate numbers are corrected pixel locations on the CCD camera; center of direct beam is near middle of right-hand edge of image (Table 2). Prominent rings of sharp diffractions are suggest that the target consists of randomly oriented grains of one or more minerals. [b] Integration of this image into d values (by FIT2D® [19]). The peaks of this 'powder-X-ray diffraction pattern' can be attributed to quartz (Qz), orthopyroxene (Px), anorthite feldspar (An), and possibly tridymite (Tr). These mineral assignments are consistent with electron microprobe chemical analyses.

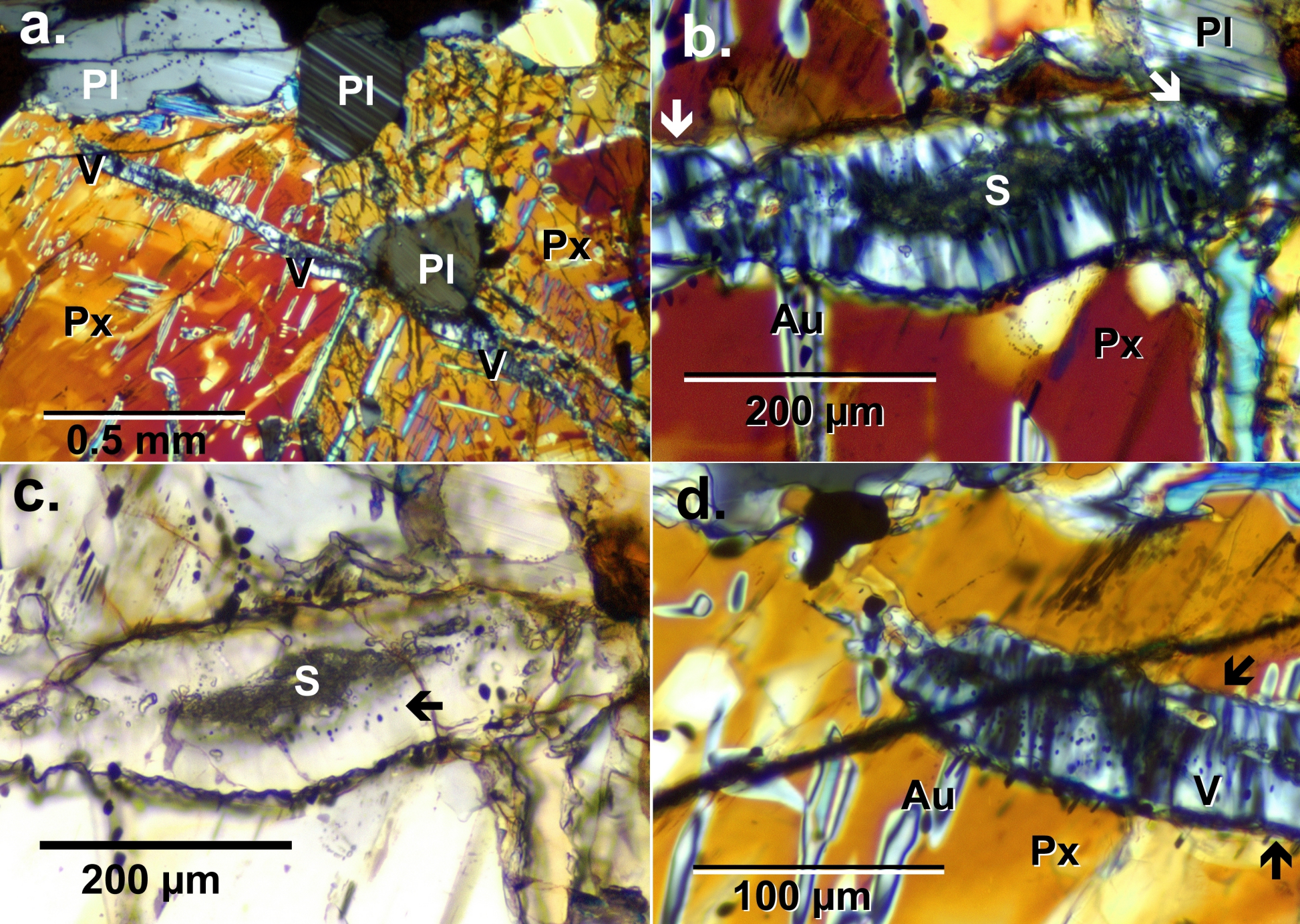
a.
Pl
Pl
V
V
Pl
Px
Px
V
0.5 mm
b.
Pl
S
Au
Px
200 µm
c.
S
200 µm
d.
Au
V
Px
100 µm

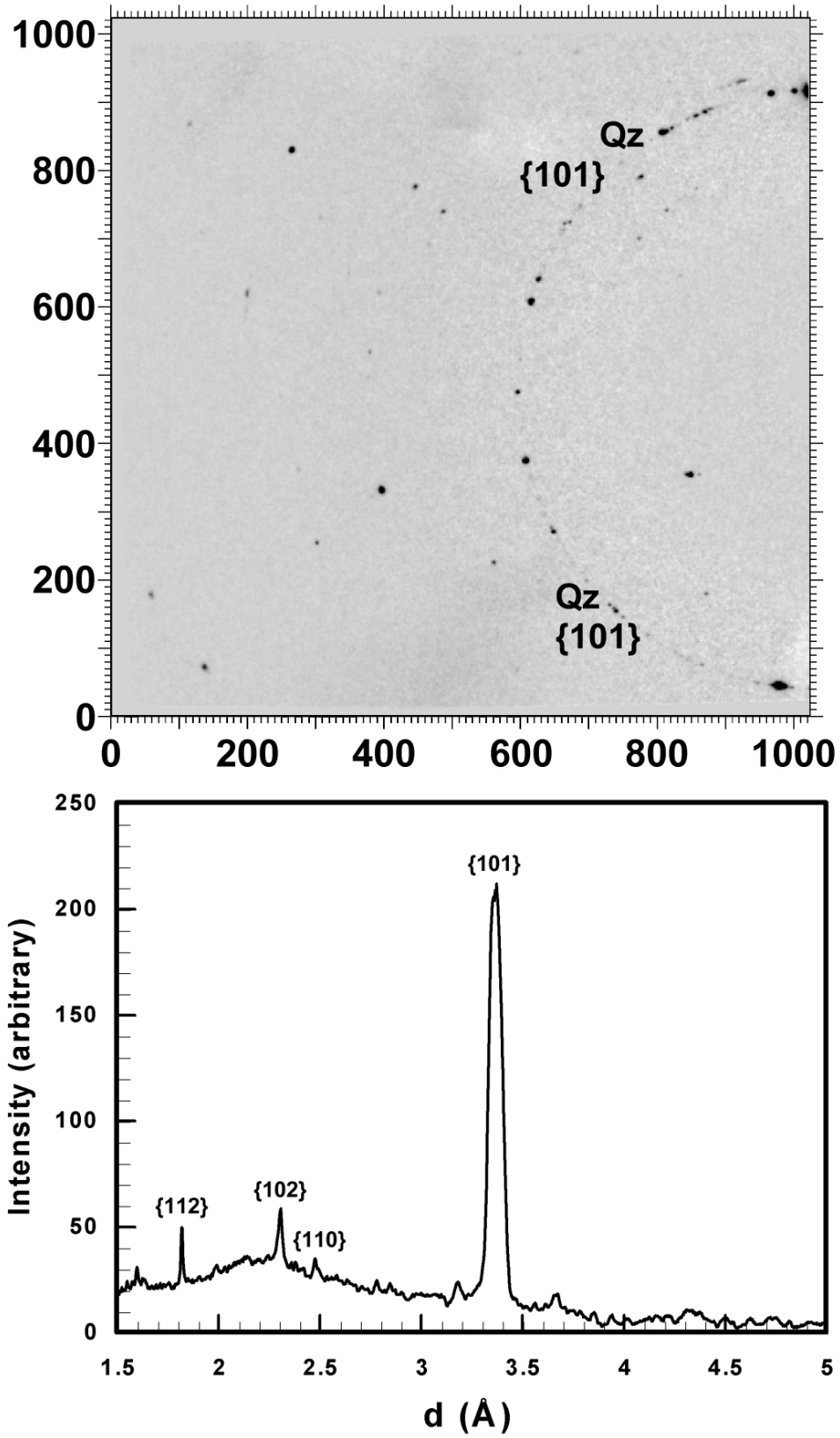
1000
800
600
400
200
0
0
200
400
600
800
1000
Qz
{101}
Qz
{101}
250
200
150
100
50
0
Intensity (arbitrary)
{101}
{112}
{102}
{110}
1.5
2
2.5
3
3.5
4
4.5
5
d (Å)

Figure 2.

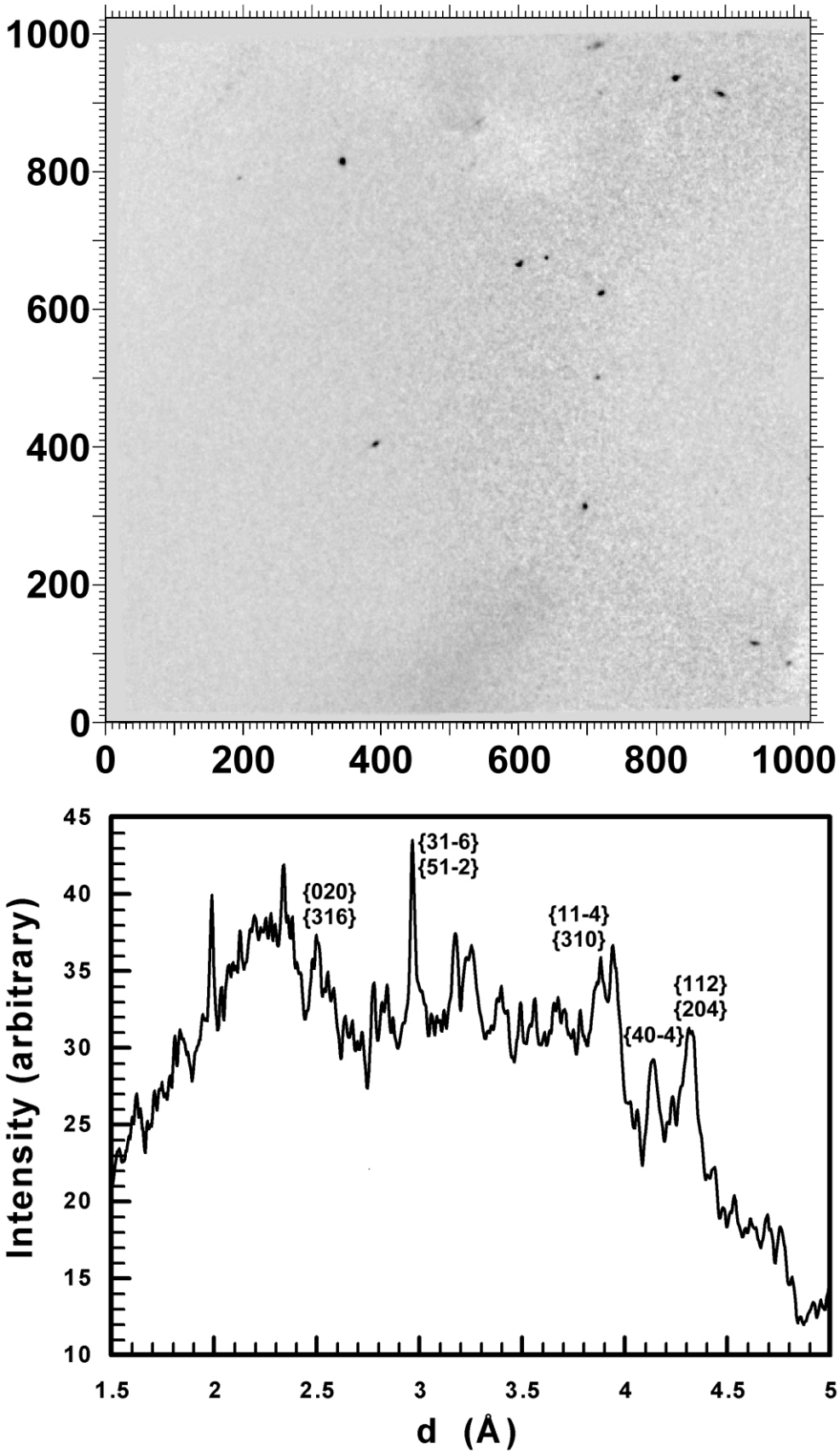
1000
800
600
400
200
0
0
200
400
600
800
1000
45
40
35
30
25
20
15
10
Intensity (arbitrary)
{020}
{316}
{31-6}
{51-2}
{11-4}
{310}
{40-4}
{112}
{204}
1.5
2
2.5
3
3.5
4
4.5
5
d (Å)

Figure 3.

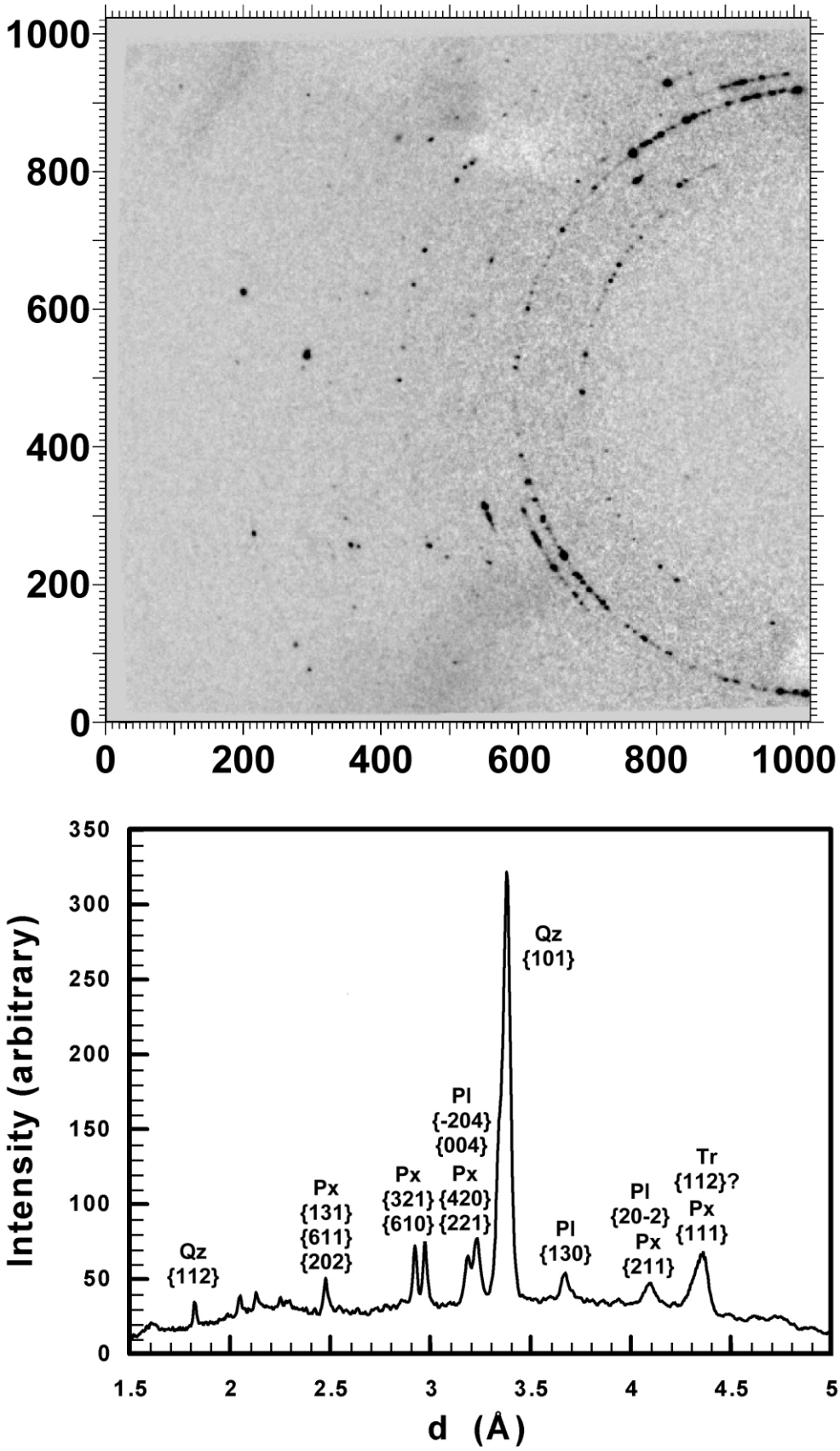
1000
800
600
400
200
0
0
200
400
600
800
1000
Intensity (arbitrary)
350
300
250
200
150
100
50
0
Qz
{112}
Px
{131}
{611}
{202}
Px
{321}
{610}
Pl
{-204}
{004}
Px
{420}
{221}
Qz
{101}
Pl
{130}
Pl
{20-2}
Px
{211}
Tr
{112}?
Px
{111}
1.5
2
2.5
3
3.5
4
4.5
5
d (Å)

Figure 4.